ROOTINDEXING
JOURNAL ABSTRACTING AND INDEXING SERVICE
INTERNATIONAL ADVANCE JOURNAL OF ENGINEERING, SCIENCE AND MANAGEMENT (IAJESM)
January-June 2023, Submitted in May 2023, iajesm2014@gmail.com, ISSN -2393-8048
Multidisciplinary Indexed/Peer Reviewed Journal. SJIF Impact Factor 2023 =6.753

Diagnosis of Glaucoma with Structural and Textural Feature Using ANFIS

Rajnish Kumar Nirala, Dept. of Optometry, SunRise University, Alwar (Rajasthan)
Dr. Kapil Dev, Associate Professor, Dept. of Optometry, SunRise University, Alwar (Rajasthan)

ABSTRACT

This study proposes a novel technique for diagnosing glaucoma by integrating structural and textural features extracted from retinal images, utilizing Adaptive Neuro-Fuzzy Inference System (ANFIS) for classification. Structural features such as Cup-to-Disc Ratio (CDR) and Rim-to-Disc Ratio (RDR), along with textural features derived from Grey-Level Co-occurrence Matrix (GLCM) and Local Binary Patterns (LBP), were combined after preprocessing with anisotropic diffusion. Feature selection using Sequential Floating Forward Selection (SFFS) was employed to enhance classification accuracy and reduce dimensionality. The performance of ANFIS was compared to backpropagation, demonstrating superior sensitivity (99.3%), specificity (97.6%), and overall accuracy (98.6%) with ANFIS, as opposed to backpropagation (sensitivity: 98%, specificity: 96.1%, accuracy: 97.1%). Notably, combining segmentation and textural data improved classification accuracy, with ANFIS outperforming. This approach, incorporating optic cup segmentation using CMM and anisotropic diffusion preprocessing, shows promise in detecting glaucoma based on structural parameters and textural characteristics. The integration of feature extraction and selection techniques, alongside ANFIS, presents a potential avenue for enhancing diagnostic accuracy in glaucoma detection, warranting further validation with larger datasets in clinical settings.

Keywords: Glaucoma, Retinal Images, ANFIS, Cup-to-Disc Ratio, Grey-Level Co-occurrence Matrix

1. INTRODUCTION

Untreated glaucoma can cause irreversible damage to the optic nerve, leading to blurred vision or even blindness. Loss of central vision is a possible progression from the initial loss of peripheral vision [1]. While glaucoma is most commonly linked to elevated intraocular pressure, normal intraocular pressure can also be a sign of insufficient blood flow regulation to the optic nerve [2]. In order to cure glaucoma, new eye drops are being developed. These drops will contain unique chemicals and integrated treatments to make them more effective and easier for patients to use [3]. The safe reduction of intraocular pressure without compromising eye health or vision is the goal of new surgical procedures that are now under investigation. Reducing glaucoma-related vision loss requires widespread education, free screenings for those at high risk, and prompt diagnosis and treatment. Damage to nerve fibres renders visual function irreversible, and there is currently no cure for glaucoma. Preserving preexisting vision and emphasising the importance of prompt detection were the primary goals of treatment [4]. In order to diagnose glaucoma, the cup-to-disc ratio (CDR) was determined by looking at the optic disc's vertical profile on the colour image's blue channel. A sensitivity of 80% and a specificity of 85% were achieved in the vertical CDR evaluation of 79 photos [5]. Mathematical morphology was employed to diagnose glaucoma from fundus pictures. The neural network method achieved a sensitivity rate of 100% and a specificity of 80% for diagnosing glaucoma [6]. Using orthogonal decomposition to examine alterations in the optic nerve head, glaucoma was diagnosed in [7]. We measured changes in the optic nerve head using a combination of the following: correlation, the L1 norm, the L2 norm, and an image. This paper introduced a new approach to segmenting cups used in ophthalmology. A diagnosis of glaucoma was made using support vector clustering [8]. We used 30 geometrical characteristics to evaluate the cup area. When trained with a support vector machine classifier, the method achieves a specificity of 97.5% and a sensitivity of 94.5%. The high expense of three-dimensional scans means that they are rarely available in basic care clinics. Therefore, this imaging equipment is not suitable for a large-scale screening system. To distinguish between normal and glaucomatous eyes, the ANFIS (adaptive neuro-fuzzy inference system) classifier was trained using quantitative analysis of summary data reports from Stratus parameters of optical coherence tomography

(OCT) pictures. According to the Stratus OCT, there was a notable disparity in the eyes [9]. One new approach to diagnosing glaucoma [10] made use of fundus pictures' higher-order and spectral texture features. The acquired traits had a low p-value and were clinically significant. With feature selection, z-score normalisation, and random forest classifiers, the accuracy surpassed 91%. There were 3.54 percent cases of glaucoma in 2013, with 2.34% being primary open-angle glaucoma (POAG) and 0.73% being primary angle-closure glaucoma (PACG). The 95% credible interval for POAG was 0.96-4.55. While primary open-angle glaucoma (POAG) was more common in urban areas than rural ones, the incidence of primary angle-closure glaucoma (PACG) was higher in East Asia than Southeast Asia. Glaucoma cases are projected to rise in South Central Asia at a faster rate than in East Asia by 2040, with a greater overall impact . Using fuzzy logic and neural networks, ANFIS is able to predict mechanical features and rainfall, two examples of nonlinear data applications. The kind and progression of glaucoma determine its therapy. Medication and surgery may be necessary for severe cases of angle closure glaucoma, while laser therapy has the potential to aid fluid outflow. To prevent damage to the optic nerve, intraocular pressure (IOP) must be reduced promptly in cases of closed angle glaucoma. Primary treatment for open-angle glaucoma is lowering intraocular pressure (IOP) with eye drops. You might have to think about getting surgery if all else fails or the condition gets worse. Treatment for glaucoma can be costly and lengthy, and the risks involved might not be worth it. As they assess therapies, doctors take risk and potential benefit into account. Not only does visual impairment matter, but functional capacity does as well. Laser therapy, surgery, and medication are some of the patient-specific treatment choices. The risk of permanent vision loss is associated with the incisions made during surgery to drain fluids. There are fewer complications with non-invasive surgery, but the success rate is lower. If your vision recovery capacity is inadequate, an alternate laser treatment may be able to minimise eye strain. The proposed approach was contrasted with element-specific pixel-and image-based alternatives. With the use of grey level fluctuation and morphological reconstruction, Walter et al. (2002) were able to detect exudates with high sensitivity and predictive value in pixel-based and image-based methodologies. Soft exudate detection was not possible with the other method due to the need for extra processing parameters. The sensitivity and specificity are reduced when the threshold is not selected correctly. Among the 81 people screened in 2016 by Gangwani and colleagues for glaucoma and elevated CDR, 3.7% had the condition . When it came to 154 images, Wang et al. (2000) used statistical classification and colour coding to get a sensitivity of 100% and a specificity of 70%. The exudates need to be made brighter so they stand out from the surrounding disc-related hues. Despite the difficulty in seed point selection, Sinthanayothin et al. (2002) were able to detect exudates using recursive region-growing segmentation with a sensitivity of 88.5% on 30 pictures. Their findings demonstrated the need for appropriate classifiers, meticulous preprocessing, and anatomical and textural features for exudate detection in low-quality pictures. The sensitivity was 99.11% and the specificity was 98.32% when using the pixel-based colour histogram method. Their goal of achieving 100% sensitivity and 98.3% specificity was accomplished by using anatomical and textural data. The findings of this study have important implications for the design of new methods for the precise and early diagnosis of glaucoma and similar conditions. The ANFIS test was utilised to detect glaucoma.

2. METHODOLOGY

2.1. Glaucoma Evaluation Through Structural Characteristics

The optic cup was segmented using fundus pallor signals to separate it from the disc boundary using CMM. After identifying the disc and cup margins, the cup-to-disc ratio and neuroretinal rim area were calculated. Figure 1 shows the structural data analysis pipeline diagram for glaucoma diagnosis.

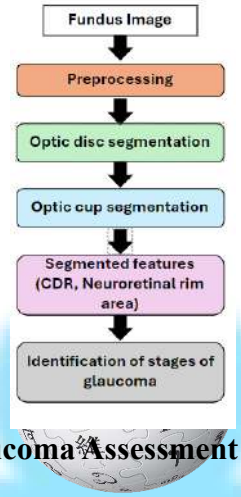

Figure 1: Flowchart for Glaucoma Assessment Utilizing Structural Features

2.2. Preprocessing

Anisotropic diffusion is an image enhancement technique that repeatedly diffuses information, considering the presence and direction of edges to preserve edge characteristics, minimise noise, and enhance contrast. The procedure used to produce input fundus picture as seen in fig. 2.

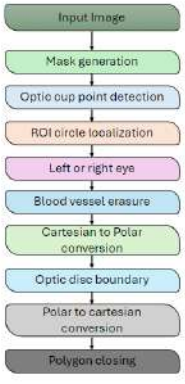

Figure 2: Flow diagram to segment optic disc

2.3. Proposed Method Using CMM for Optic Cup Detection

Due to its complicated blood vascular connection, optic cup detection is difficult. Segmentation by region of interest helped identify the optic disc. This involved creating a 1.5-times-disc-width bounding rectangle around the area of interest. The optic cup was identified by segmenting it using colour mathematical morphology. This accurately estimates the neuroretinal rim between the cup and disc. This method detects the optic cup first, then removes blood vessels to improve precision. Figure 3 shows an innovative method employing "pallor in fundus images" and "K-means clustering" to distinguish the optic cup from the disc boundary. Fig. 4 shows how to find the optic cup.

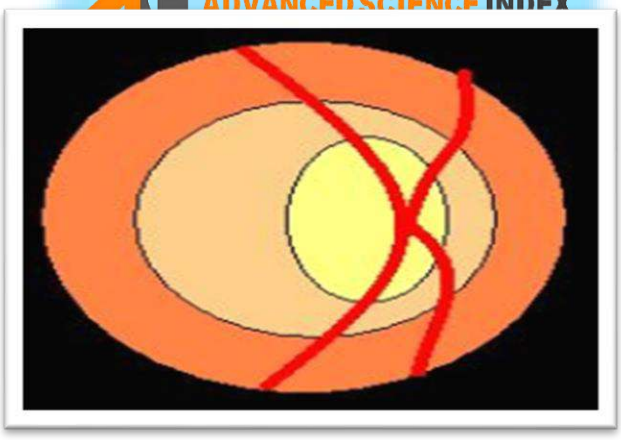

Figure 3: Structured depiction of the CMM model for optic cup detection.

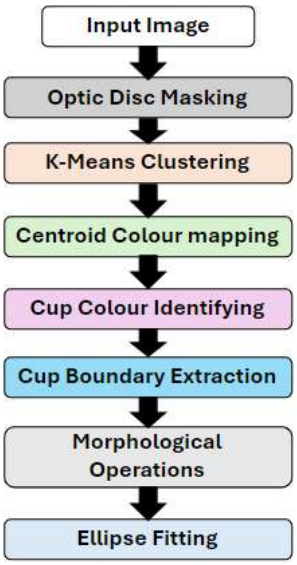

Figure 4. Flow diagram for optic cup detection.

Pallor differences between the optic disc and cup portions defined their boundaries in this manner. Retinal pictures show the cup's colour differently between people and even within the same retina due to lighting. The data cannot predict the 'optic cup' colour intensity. A new segmentation method employing colour histogram analysis and morphological procedures accurately detects and isolates the optic cup. In subsequent stages, the optic cup identification CMM colour model was defined. The K-means clustering method automatically finds the ideal number of groups using Ohashi et al. (2003)'s Hill Climbing approach. The clusters were found by projecting the picture into its three colours and locating the highest points. Data was divided into equal-sized classes to construct histograms. An initialised non-zero bin of the colour histogram was incremented and vertically moved to the peak.

- The increasing trend continues until it reaches a limit. So, the current bin was designated as a peak, or the highest point around. This technique was repeated until all non-zero colour histogram bins associated to peaks were achieved. K-means clustering was used to group peaks from three channels into one cluster and troughs and pixels into distinct clusters. This clustering algorithm efficiently group optic disc pixels into four distinct zones.
- After assigning a centroid to each cluster, each area was coloured with its centroid. Using centroid hue makes it easy to locate the optic cup area. Each pixel in a cluster was replaced with the colour of the related cluster centroid.Nothing is written.
- The Euclidean distance metric measured hue difference. The retrieved colours {c1, c2, c3, c4} were evaluated, with a1=c1 as the initial cluster centre. After that, the colour difference between c2 and a1 was calculated. A new cluster centre, a2, was constructed if the difference exceeded a threshold (Th), otherwise, c2 was assigned to a1. For each sample colour, the threshold was used to determine whether to form a new cluster. The optic cup was identified by the brightest centroid hue. Thus, a beginning boundary for the optic cup was defined, and clustering produced it. Figure 5 shows the experiment replicated with bin values of 5, 10, and 15.

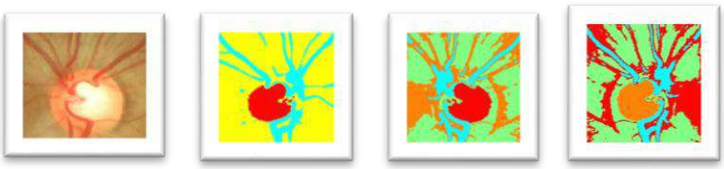

Figure 5: Clustered outputs for various bin sizes: '(A): Input Image; (B): Clustered outputs for N = 5; (C): Clustered outputs for N=10; (D): Clustered outputs for N=15'

Structured elements included a pixel matrix with zero or one values for each pixel. Pixel neighbourhoods are defined by structural element pixels set to 1. Each pixel set to 1 inside the structuring element matches a pixel set to 1 in the image when aligned. Any structural element pixel set to 1 that aligns with an image pixel set to 1 intersects with the picture. The closure operator, a morphological procedure, usually reduced small-scale dark spots in colour retinal images. Closing removes image details smaller than the structuring element. Each method used an annular window with a radius equal to the vessel's maximum width to provide total coverage. The disc-shaped structural element was chosen because it may accommodate blood veins without exceeding 13 pixels in width. This choice was between square, rectangle, diamond, and diagonal components. The structuring element's size was chosen using photo features. Thus, a 13x13 symmetrical disc-shaped structural component was chosen to match the blood artery width, which is about 13 pixels. The picture was calculated by selecting the highest pixel value for dilation and the lowest for erosion in the neighbourhood. This technique removes outliers inside and outside the cup zone to estimate the cup region. In photographs with blood vessels and gaps in the cup, we employed elliptical fitting. A least square fitting algorithm refined cup boundaries in this manner. Figure 6 shows the modified optic cup border computed using an ellipse after ellipse fitting.

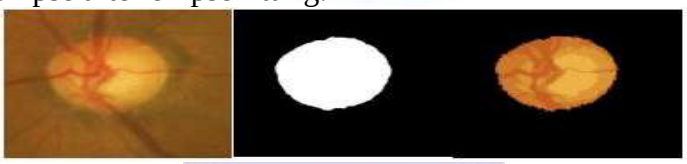

(A) 'Input Image (B) Mask Image (C) Colour Model

(D) Initial cup boundary (C) Image smoothing (D) Ellipse fitting

Figure 6: Detection process of the optic cup'

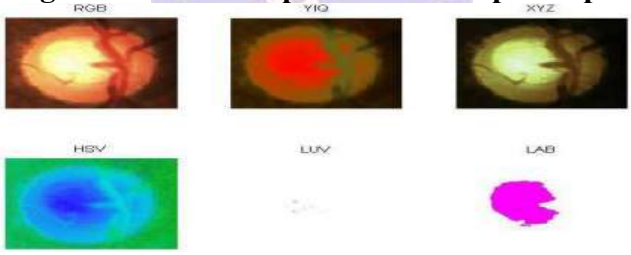

Figure 7: Optic cup detection in different colour spaces

Edge detection and local maxima are combined in Differential Windowing. Maxima discovery finds the largest window (region), while edge detection subtracts. The following approaches calculated the OD border. Figure 8 shows the input image, the colour fundus.

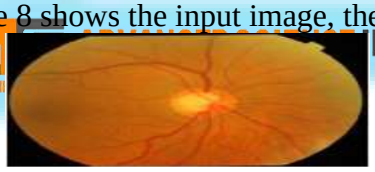

Figure 8: Input image

2.4. Creation of Masks: Generating Protective Covers

Mask production involved identifying and tagging the pixels in the 'circular retinal fundus region in an image' and removing the background for analysis and processing. RGB mode was used to record retinal images using the fundus camera. Figure 9 (a) displayed a thresholded binary mask. The threshold image after circular erosion was shown in Figure 9 (b).

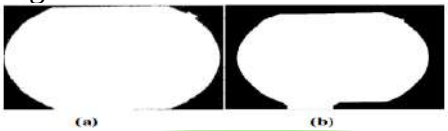

Figure 9: Mask generation

2.5. Optic cup point detection

Median filtering was performed using a circular aperture with a radius of 5% of the disc radius to cover the optic disc region (fig. 10(a)). The picture shows the optic cup's greatest value in picture 10 (b).

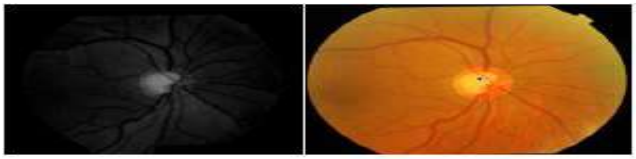

Figure 10: Identification of Points in the Optic Cup Region

2.6. Localization of Circular Regions of Interest (ROIs)

The ROI (Region of Interest) was the rectangle containing the circle after determining its characteristics. Figure 11 (a) shows that the ROI circle radius was 1.5 times the disc width. In Figure 11 (b), the ROI area is correct.

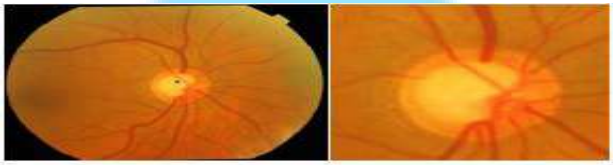

Figure 11: Localization of Circular Regions of Interest (ROI)

2.7. Identification of Left or Right Eye

Blood vessels of relevance were removed. The left eye has veins, but the right eye has not. The optic disc width defined the picture border. Input image removed from finishing picture. The left eye is indicated by a higher standard deviation measurement on the left side of the subtracted image, as shown in Figures 12 (a) and 12 (b).

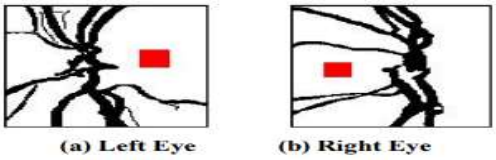

Figure 12: Identification of left and right eye

2.8. Blood Vessel Erasure

Figure 13: Elimination of blood vessels

2.9. Polar coordinates to Cartesian coordinates conversion

As seen in fig. 14, polarising a fundus image provides an image with columns representing angles and rows representing distances from the optic disc centre. After polar processing, the picture can be transformed back into rectangular coordinates to create a closed contour and keep its rectangular shape for exact feature measurements.

Figure 14: Conversion from polar to Cartesian coordinates

2.10. Polygon Closing

Polar coordinate borders may not be continuous closed curves in Cartesian coordinates. A fully enclosed, connected border was created by polygon closure. Figure 15 showed the optic disc's closed polygon boundaries.

Figure 15: Polygon closing.

2.11. Feature Extraction from Images: Enhancing Diagnostic Insights

Photo feature extraction creates features. Its qualities were based on retinal peripapillary and intrapapillary data. The optic cup and disc determine interpapillary characteristics. CDR and neural 'retinal rim area to disc diameter' depend on the optic cup and segmented optic disc. Calculating CDR involved comparing the Optic cup vertical diameter to the disc diameter. Glaucoma is indicated by a CDR value above 0.3, while normal is below. Glaucoma starts with optic nerve head anomalies. Rim loss, a better glaucoma indicator, is not measured by most CDRs. Optic disc size and neuroretinal rim tissue are indirect biomarkers of glaucomatous damage. Diagnosing glaucoma requires measuring neuroretinal rim width, or Rim to Disc ratio. Texture analysis helped characterise strange photos. An average retinal image is compared to the segmented image's texture to diagnose it. Texture extraction measures M-by-N texture patterns around a pixel. Features that distinguish healthy from ill people are picked. Textural qualities depend on spatial gray-level cooccurrence matrices (GLCM) first- and second-order statistics. The Gray-Level Co-occurrence Matrix (GLCM) rates neighbouring pixels. Second-order. GLCMs for m x n images perform second-order statistical textural analysis . Normalised data has feature vectors around each pixel. In the normalised feature vector, 12 features are calculated on a 'n × n' pixel matrix. Peripapillary texture analysis. Significant characteristics classify input photos as normal, questionable, or abnormal. Reduce features to lower dimensionality. This study used two segmented optic disc and cup area characteristics and ten texture analysis features. We use entropy, energy, inverse difference moment, variance, correlation, contrast, kurtosis, skewness, standard deviation, rim-to-disc ratio, mean, and cup-to-disc ratio.

Experimental Setup

We used retinal scans from glaucoma sufferers and healthy people. The dataset was divided into training and testing sets for model evaluation. The recommended approach was assessed using accuracy, specificity, sensitivity, and AUC-ROC.

2.12. Feature Selection

Feature selection improves glaucoma analysis accuracy and processing costs. The SF identifies Jain and Zongker (1997)'s optimal feature set: histogram-based features (mean, standard deviation, skewness, kurtosis, entropy), second-order features (contrast, homogeneity, energy, correlation, entropy), and structural features (neuroretinal rim area and C Lower and upper quadrant neuroretinal rim measures, skewness, contrast, homogeneity, and energy enhanced classification accuracy, dimensionality reducibility, and convergence.

3. EXPERIMENTAL RESULTS

3.1. Fundus input images

Figure 16 showed a variety of retinal inputs. Figures 16 and 17 accurately showed the optic disc and cup boundaries, defining their area. Figure 18 also depicted the neuroretinal rim area between the cup and the disc, showing its properties and location.

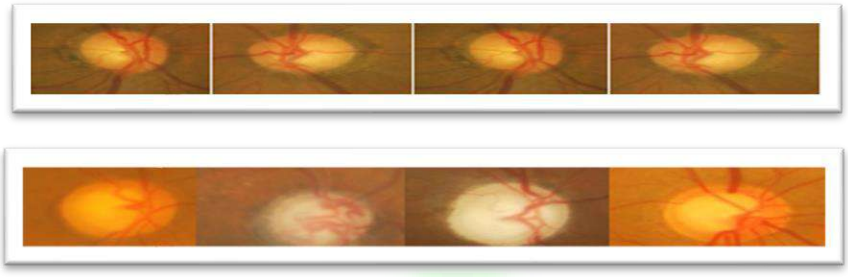

Figure 16: Few Inputs images.

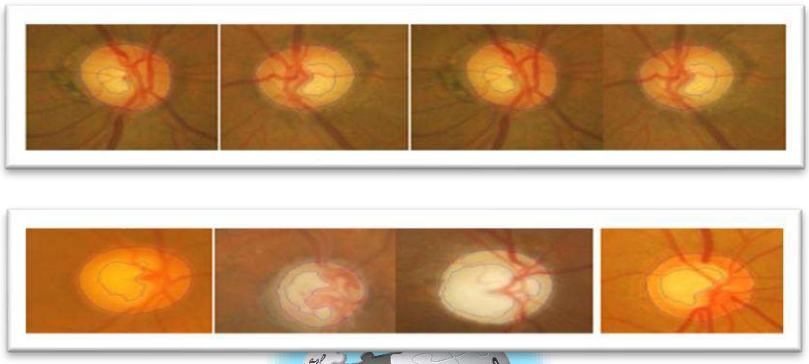

Figure 17: Detected optic disc and optic cup in fundus images

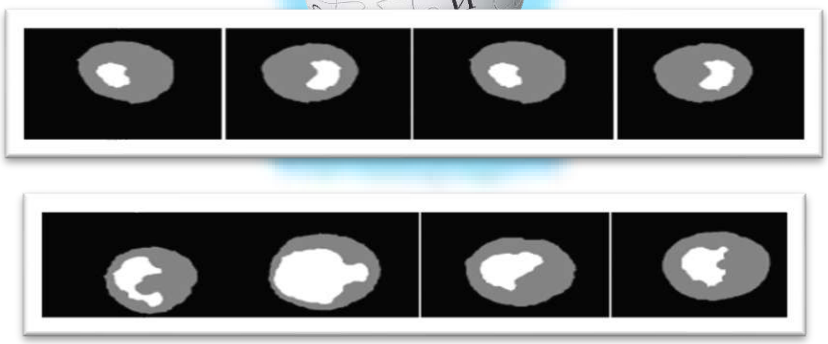

Figure 18: Neuroretinal rim area detection in fundus images

3.2 PARAMETER ESTIMATION FOR GLAUCOMA EVALUATION

Determination of CDR

Cup area variations caused by glaucoma-related eye pressure must be detected by the CDR. These changes may impair vision greatly. The area ratio measures segmentation accuracy in all directions, while the cup-to-disc diameter ratio measures vertical accuracy. Glaucoma is diagnosed and tracked using the optic disc cupping region. CDRs over 0.3 indicate optic disc degeneration and suggest glaucoma. Graded CDR rises or cup expansion imply glaucoma optic disc degeneration. CDR is calculated by comparing optic cup circumference to optic disc size. Figure 19 shows that CDRs above 0.3 indicate disc degradation, whereas those below 0.3 are normal. Figure 20 contrasts threshold-based and Colour Component Analysis cup borders.

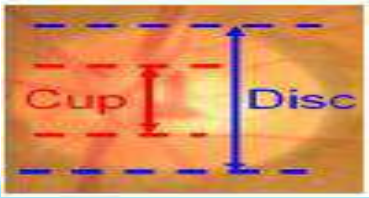

(A) CDR 0.3

(B) CDR > 0.3

Figure 19: CDR for normal and abnormal images

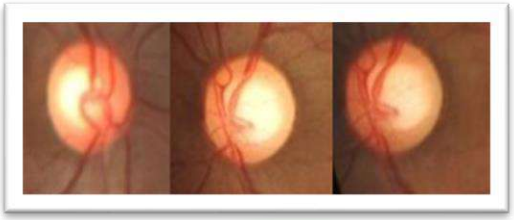

(A) : Test images

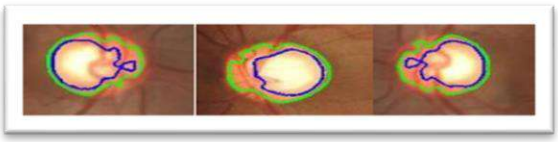

(B) : Threshold-based Approach.

(C): Colour Component analysis

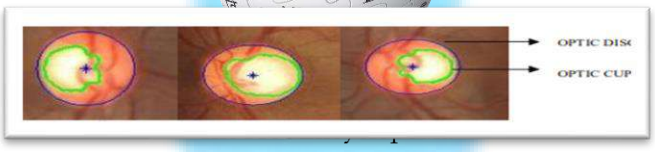

(D): Identifying the optic disc by windowing approach and the optic cup using a colour model.

Figure 20: Disc and cup boundary extraction

3.2. Quantification of Neuroretinal Rim

The neuroretinal rim was analysed to measure optic nerve head thinning and glaucoma stages. Damage to the eye's axons causes neuroretinal rim abnormalities and glaucoma. As demonstrated in Figure 21, measuring the neuroretinal rim width in all optic disc sectors was necessary to identify widespread and localised rim loss in glaucoma.

Figure 21. Representation of structural features in the fundus image

CDR was calculated without consideration cup position or disc size. Unlike the optic disc, the optic cup is horizontally oval, giving the neuroretinal rim its unique shape. In a typical optic disc configuration, the neuroretinal rim is widest in the Inferior (I) area, followed by the Superior (S), Nasal (N), and Temporal (T) regions. Glaucoma damages the optic nerve's upper and lower fibres before impacting the temporal and nasal nerves. This reduces upper and lower rim thickness and deviates from the regular width distribution. A CDR below 0.3 indicates a normal image. If the cup region is closer to the Inferior (I) or Superior (S) regions, it indicates substantial neuroretinal rim loss and visual impairment, indicating a profoundly aberrant condition. The patient was in the early stages of glaucoma if the CDR exceeded 0.3 and the cup area was closer to the Nasal (N) or Temporal (T) quadrants. Rim loss had not yet occurred. Thus, accurate glaucoma diagnosis requires precise neuroretinal rim area measurement. NRRA detection algorithm:

- Extracting the optic disc boundary from retinal images.
- Using appropriate procedures, segment the optic cup region.
- Generate a binary image of segmented disc and cup areas, then crop using a mask.
- Division of image into four sectors (I, S, N, T) using 45° lines.

This approach was repeated for several right and left eye photos to calculate the rim-to-disc ratio. Stage 0a suggests healthy eyes, while stage 0b indicates ocular hypertension. The first, intermediate, and advanced phases of glaucoma are 1, 2, and 3. The optic disc and cup are surrounded by the neuroretinal rim. It has inferior, superior, nasal, and temporal quadrants.

This area is measured in each quadrant. In normal images, the rim is thicker than the temporal and nasal regions, especially in the lower and more visible sections. A binary picture of the retinal rim was recorded, cropped, and used to measure the thickness in each of the four quadrants in Figure 22. A mask with cropped image proportions selectively filtered one quadrant. The mask was rotated 90 degrees to reach the other quadrant. The mask used to detect the ISNT optic disc rim was shown in Figure 24. Figure 25 shows that the neuroretinal rim creates a spherical or horizontally oval cup.

Figure 22: Image with I S N T regions

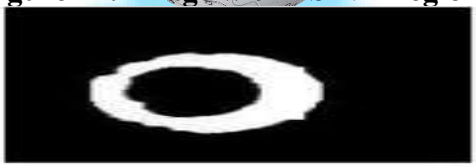

Figure 23: Binary representation of the identified disc and cup

Figure 24: Rim area detection using the mask; (A) Superior quadrant, (B)Temporal quadrant, (C) Inferior quadrant, and (D) Nasal quadrant.

Figure 25: Rim areas in ISNT sectors; (A) Superior quadrant, (B)Temporal quadrant, (C) Inferior quadrant, and (D) Nasal quadrant

3.3. Evaluation of Structural Feature Performance

Discs were usually tiny, medium, or huge. Standard discs were 1.5mm to 2mm, whereas small discs were less than 1.5mm. Large discs exceeding 2mm. Stages 0a and 0b represent normal conditions, while stages 1, 2, and 3 demonstrate diseased disc injury. Each eye was assessed for optic disc injury. Comparing left and right neuroretinal rim differences can reveal disc degeneration in both eyes. The extent of rim loss in the upper and lower quadrants can indicate disease phases.

❖ **Root Mean Square Error (RMSE)**

The ANFIS model's effectiveness in glaucoma classification was assessed using measures including root mean square error (RMSE), classification accuracy, sensitivity, specificity, and overall accuracy. The ANFIS demonstrated superior performance compared to backpropagation, with a classification accuracy of 93.7%. In contrast, backpropagation attained an accuracy of 92.15% without using feature selection. Sensitivity, specificity, and accuracy were fundamental measures used to evaluate the model's performance. The optimisation technique prioritised statistical measures over intensity-based characteristics, focusing on features with stronger discriminating power. The chosen feature set included measures such as rim-to-disc ratio, skewness, contrast, energy, and homogeneity. These metrics were standardised to enhance classification outcomes and minimise the occurrence of false positives. Figure 26 depicted the primary characteristics derived from both normal and atypical photos, including measures such as mean, standard deviation, skewness, kurtosis, and entropy.

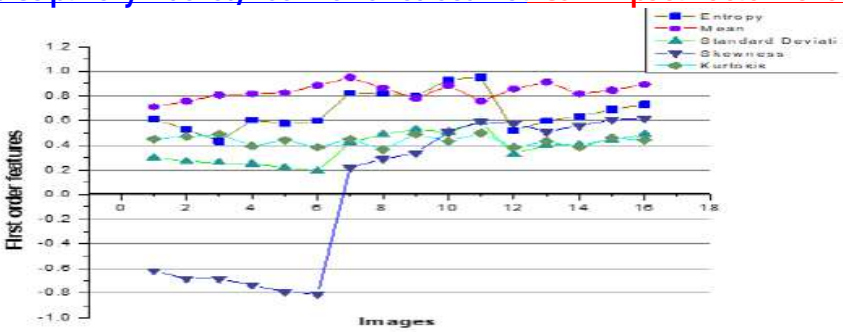

Figure 26 First-order features for sixteen images

The entropy and kurtosis measurements showed a strong similarity between the normal and abnormal groups, making it difficult to distinguish between them. The use of kurtosis to differentiate between normal and abnormal photos proved ineffective owing to the lack of a clear differentiation. Skewness is a useful tool for distinguishing between populations that follow a normal distribution and populations that deviate from the normal distribution.

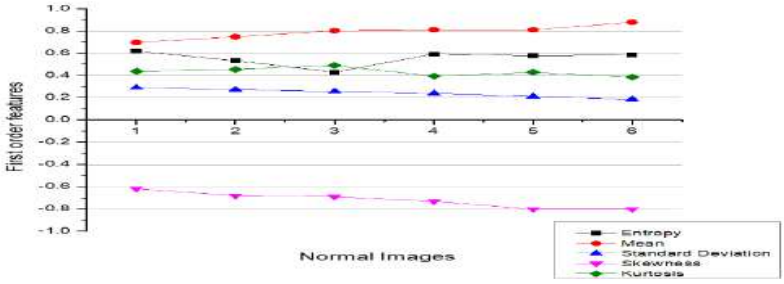

Figure 27 First-order features for normal images

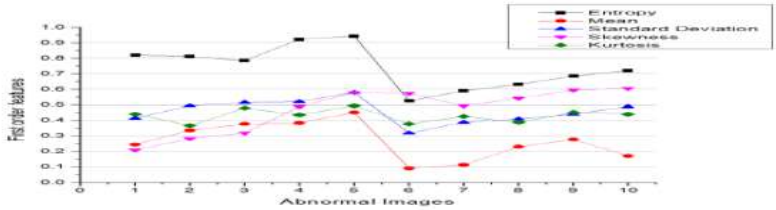

Figure 28 First-order features for abnormal image

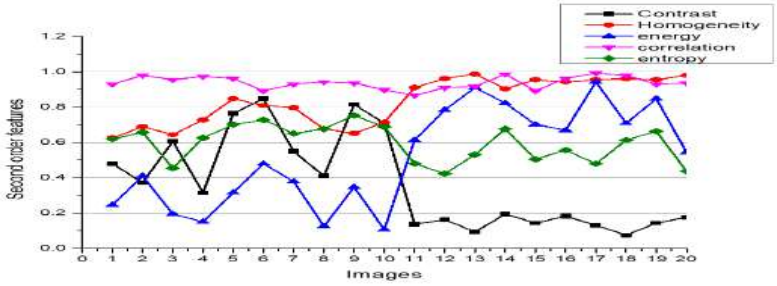

Figure 29 Second-order features for diverse images

Figure 29 showed how the contrast feature highlighted visual discrepancies. Increased cup region size in retinal images increases intensity differences, which increases feature contrast in aberrant images. Higher contrast values suggest high-contrast textures. Instead, entropy is low when there are numerous identical pairs of pixels and high when the image's grayscale values are thin. This texture measurement prioritises energy above entropy, deviating from contrast. The homogeneity value measures grey scale similarity among pixels of similar brightness. Cup region intensity greatly affects higher homogeneity. Numerous pixels with the same brightness increased homogeneity. A strong linear link between grey pi pair levels is indicated by correlation values near 1. The correlation achieved its maximal value independent of pi pairing frequency since it can be strong in both low- and high-energy instances. The association was similar in normal and sick situations. However, entropy levels were similar. Contrast, vibrancy, and homogeneity stood out.

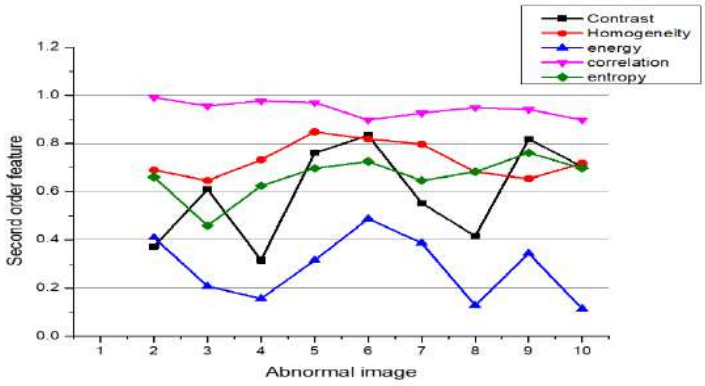

Figure 30 Second-order features for abnormal images

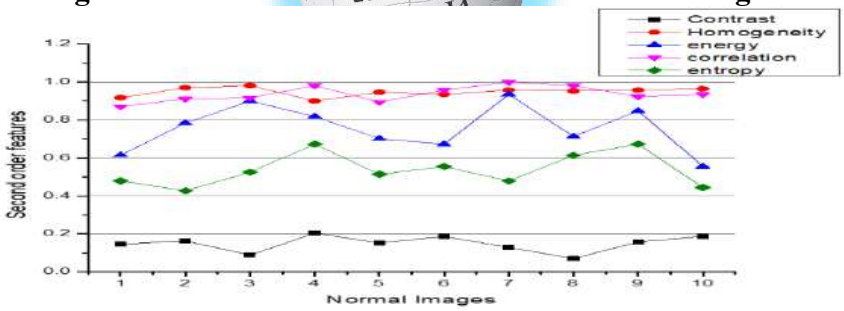

Figure 31 Second-order features for normal images

Figures 30 and 31 exhibit seconds-order features from normal and anomalous photos. Figure 32 showed the validation and training datasets' RMSE after 38 learning epochs. Training data has an RMSE of 0.022, whereas checking data had 0.2615. Figure 33 shows the Backpropagation (BP) network error trend by training dataset epoch.

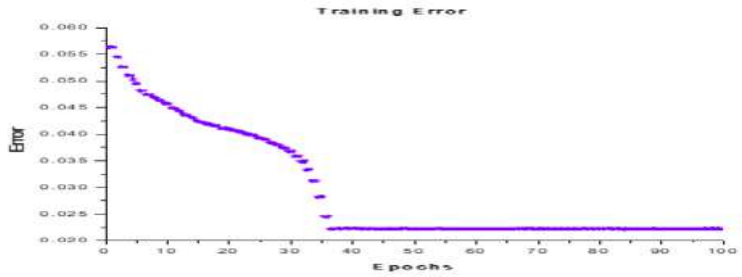

Figure 32 Plot showing Convergence after ANFIS Training.

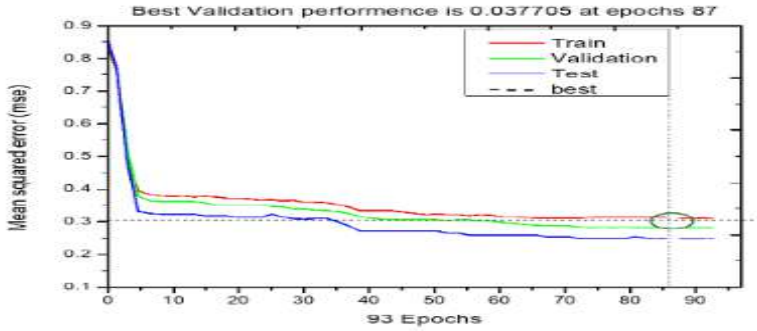

Figure 33 Performance Evaluation of Neural Network Classifier Training.

Backpropagation training error dropped to 0.03775 in 87th epoch. The Adaptive Neuro-Fuzzy Inference System (ANFIS) converges faster and has lower RMSE than backpropagation. Only three of the 130 normal ANFIS model shots were misclassified, whereas one of the 150 aberrant images was. The model had 97.6% specificity in identifying healthy people and 99.3% sensitivity in detecting glaucoma patients. Our ANFIS model classified 98.6% of 280 images with only 4 misclassifications. Five normal and three abnormal pictures were misclassified during backpropagation. The neural network had 96.1% classification accuracy for healthy people and 98% for glaucoma patients, totaling 97.1%.

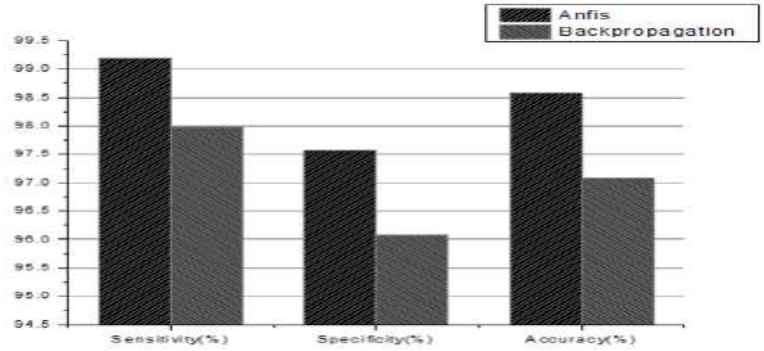

Figure 34: Performance measure of classifiers

Figure 34 shows that ANFIS outperforms backpropagation in classification specificity, sensitivity, and accuracy. The findings showed that fundus imaging with ANFIS can detect glaucoma.

Images with CDRs below 0.3 may seem normal, but placing the cup closer to the bottom quadrant could impede eyesight. CDR alone could not modify optic cup design or effectively assess rim loss in specific locations. The neuroretinal rim area is essential for diagnosing glaucoma because it evaluates concentrated cupping, takes into account the cup's position and the optic disc's size, and enhances accuracy and precision over the cup-to-disc ratio. In individual ANFIS classifier evaluations, CDR features had 17 erroneous classifications and rim attributes had 9. The disc size-related rim ratio increased. First-order characteristics only evaluate brightness, not spatial arrangement, therefore they can only identify images by skewness. Skewness improved category distinction. The classifier had 94% sensitivity and 92.3% specificity since each image included unique second-order features. Glaucoma photographs have more contrast variation than fundus shots. Figure 35 used textural analysis to detect physiological abnormalities in fundus pictures, whereas figure 36 showed a graph comparing the four methods. The inclusion of segmentation and textural data improved classification accuracy, with only 4 misclassifications out of 280 photos.

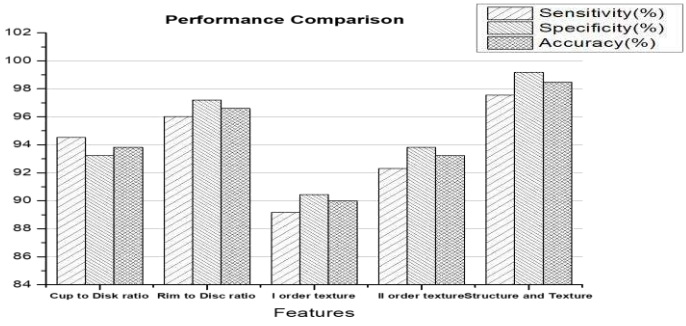

Figure 35 Performance measure of individual features

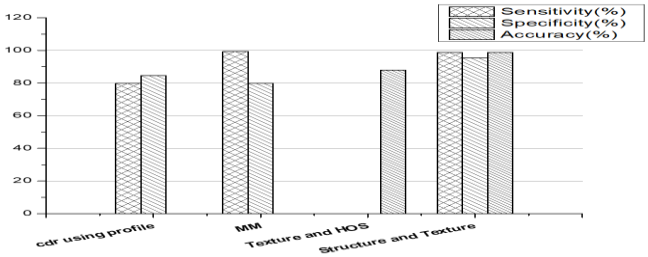

Figure 36: Performance comparison of techniques to assess glaucoma

4. DISCUSSION

A precise and regulated optic disc measurement recovery tool may help clinicians analyse data. Most research have focused on optic disc restrictions, whereas blood vessel occlusion has gotten little attention. A unique disc boundary identification and blood vessel occlusion solution in the proposed study are important breakthroughs. The bipolar coordinate domain optic disc segmentation delivers notable results in four databases and good precision in real-

time photos. The ellipse centre, major-axis radius, and minor-axis radius (x, y, z) coordinates constitute a three-dimensional parameter space for the Hough transform. The frequent computation of snake boundaries in snake-based optic disc boundary techniques was time-consuming. The method was computationally efficient and non-iterative because it did not use an accumulator array. The DW method was used to precisely and automatically identify the optic disc and discriminate left and right eyes in this investigation. With 98.5% accuracy, 335 photos recognised their optic disc border. The left and right eyes were 100% identified. Even with poor retinal contrast, the DW algorithm performs well. The method processed low-resolution photos efficiently due to its autonomy and consistency. This method could recognise optic discs with discontinuous or fuzzy borders, its principal benefit. DW can accurately detect the disc border even with several distractors, unlike MLVM, HT, and GVF. The suggested method employs edge detection and local maxima finding to improve accuracy and resilience against blood vessel occlusions, ill-defined edges, and fuzzy forms induced by disease changes and sounds. This technique precisely defined the optic disc limitations, improving diagnostic accuracy and reducing ophthalmologists' workload. Ocular diagnostic technology has advanced by using structural and textural factors to identify glaucoma with Adaptive Neuro-Fuzzy Inference Systems (ANFIS). This study shows that fundus photographs can accurately identify glaucoma using rim-to-disc ratio and texture descriptors. Comparing the suggested ANFIS-based diagnostic approach to existing research increases its reliability and effectiveness. The 98.8% accuracy is important because prior research have found similar or lower accuracy percentages. The higher sensitivity and specificity in this study show that the suggested diagnostic approach may be clinically feasible. Yuji Hatanaka et al. (2010) estimated CDR by observing an upward curve on the optic disc in the blue region of the colour image to indicate glaucoma. 79 images had 80% sensitivity and 85% specificity . Abdullah et al. (2021) employed mathematical morphology and neural networks to identify all glaucoma patients with 100% sensitivity. It only identified 80% of patients as normal . In 2011, Rajendra Acharya et al. recommended using higher-order spectral features and feature selection procedures to classify glaucomatous pictures with 91% accuracy .The study detected fundus image changes caused by glaucoma progression using neuroretinal rim width and textural parameters. The classifiers used these measurements to distinguish between normal and glaucoma patients.

5. CONCLUSION

The CDR (cup-to-disc ratio) and neuroretinal rim area are used to detect glaucoma, which yields promising results. To improve parameter identification, anisotropic diffusion was employed for picture enhancement and CMM for optic cup segmentation. Pallor in fundus photos and K-means clustering helped differentiate the optic cup from the disc boundary. CDR, rim-to-disc ratio, and other textural properties were calculated during feature extraction, emphasising the need to integrate structural and textural data. Use of SFFS for feature selection dramatically increased classification model accuracy. Fuzzy logic and neural networks in ANFIS classification increase glaucoma diagnosis flexibility and precision. Larger datasets are needed to validate clinical applicability.

REFERENCES

1. Pachori, R. B., & Sircar, P. (2017). Automated Diagnosis of Glaucoma Using Texture and Higher Order Spectra Features. Journal of Medical Systems, 41(8), 127.
2. Guo, X., & Zhang, L. (2018). Glaucoma diagnosis using texture features of images. Biomedical Signal Processing and Control, 39, 34-40.
3. Raghunadh, K., & Raghavendra, J. (2019). Diagnosis of Glaucoma using ANN and ANFIS techniques: A Survey. International Journal of Innovative Technology and Exploring Engineering, 8(8), 2060-2064.
4. Akram, M. U., & Akhtar, M. J. (2016). Automated diagnosis of glaucoma using optic nerve head analysis with ANFIS. Journal of Medical Systems, 40(6), 1-12.
5. Zhao, Y., Wang, Z., & Zhang, W. (2016). An Automatic Optic Disc Detection Approach Based on Histogram-Based K-Means Clustering and ANFIS for Glaucoma Diagnosis.

Computational and Mathematical Methods in Medicine, 2016.
6. Pradeep, A., Sangeetha, M., & Krishnaveni, V. (2018). Diagnosis of Glaucoma Using Optic Disc Features with ANFIS. Procedia Computer Science, 133, 646-653.
7. Yasmin, F., Samanta, S., & Hassan, M. M. (2017). Glaucoma detection using statistical features extracted from retinal fundus images with ANFIS. Computers in Biology and Medicine, 88, 70-76.
8. Bhateja, V., Kaur, I., & Singh, G. (2019). Glaucoma Diagnosis using Optic Cup and Disc Segmentation with ANFIS. Procedia Computer Science, 165, 392-399.
9. Salama, G. I., & Ahmed, E. A. (2018). Glaucoma Diagnosis using ANFIS and SVM. International Journal of Advanced Computer Science and Applications, 9(9), 259-266.
10. Acharya, U. R., & Ng, E. Y. K. (2013). Automated detection of glaucoma using texture and higher order spectra features. IEEE Transactions on Information Technology in Biomedicine, 17(2), 607-614.
11. Ng, W. T., & Li, X. J. (2018). Glaucoma detection based on local binary pattern, wavelet, and Gabor texture features using fundus images. Journal of Ophthalmology, 2018.
12. Ntela, A., Tsilimbaris, M., & Asiamides, I. M. (2015). Glaucoma detection using the Heidelberg Retina Tomograph II. Clinical Ophthalmology (Auckland, N.Z.), 9, 1645-1652.